Colloidal Bi-Doped Cs2Ag1–xNaxInCl6 Nanocrystals: Undercoordinated Surface Cl Ions Limit their Light Emission Efficiency

ACS MATERIALS LETTERS

www.acsmaterialsletters.org

Colloidal Bi-Doped $Cs_2Ag_{1-x}Na_xInCl_6$ Nanocrystals: Undercoordinated Surface Cl Ions Limit their Light Emission Efficiency

Baowei Zhang,[⊥] Mengjiao Wang,*[,⊥] Michele Ghini,[⊥] Angela E. M. Melcherts, Juliette Zito, Luca Goldoni, Ivan Infante, Michele Guizzardi, Francesco Scotognella, Ilka Kriegel,* Luca De Trizio,* and Liberato Manna*

Cite This: *ACS Materials Lett.* 2020, 2, 1442–1449

Read Online

ACCESS | Metrics & More | Article Recommendations | Supporting Information

ABSTRACT: Understanding and tuning the ligand shell composition in colloidal halide perovskite nanocrystals (NCs) has been done systematically only for Pb-based perovskites, while much less is known on the surface of Pb-free perovskite systems. Here, we reveal the ligand shell architecture of Bi-doped $Cs_2Ag_{1-x}Na_xInCl_6$NCs via nuclear magnetic resonance analysis. This material, in its bulk form, was found to have a photoluminescence quantum yield (PLQY) as high as 86%, a record value for halide double perovskites. Our results show that both amines and carboxylic acids are present and homogeneously distributed over the surface of the NCs. Notably, even for an optimized surface ligand coating, achieved by combining dodecanoic acid and decylamine, a maximum PLQY value of only 37% is reached, with no further improvements observed when exploiting post-synthesis ligand exchange procedures (involving Cs-oleate, different ammonium halides, thiocyanates and sulfonic acids). Our density functional theory calculations indicate that, even with the best ligands combination, a small fraction of unpassivated surface sites, namely undercoordinated Cl ions, is sufficient to create deep trap states, opposite to the case of Pb-based perovskites that exhibit much higher defect tolerance. This was corroborated by our transient absorption measurements, which showed that an ultrafast trapping of holes (most likely mediated by surface Cl-trap states) competes with their localization at the $AgCl_6$ octahedra, from where, instead, they can undergo an optically active recombination yielding the observed PL emission. Our results highlight that alternative surface passivation strategies should be devised to further optimize the PLQY of double perovskite NCs, which might include their incorporation inside inorganic shells.

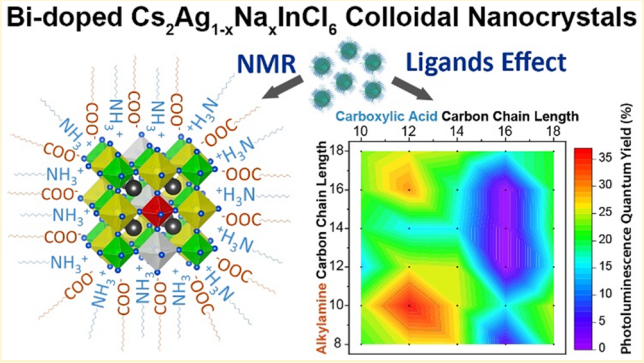

Lead halide perovskites nanocrystals (NCs) are among the most promising luminescent nanomaterials for potential applications in optoelectronic devices, such as light emitting diodes and displays.[1−4] However, the intrinsic toxicity of Pb and the poor stability of such materials under air and, in particular, moisture can limit their applications.[5] Therefore, efforts are aiming at developing non-toxic alternative perovskite NC materials featuring a bright photoluminescence (PL) and, at the same time, high stability.[6] In this regard, the so-called double perovskite (DP) NCs, having chemical formula $A_2B^+B^{3+}X_6$, have been identified as possible alternative materials. They are characterized by a 3D perovskite skeleton composed of corner-sharing $[B^+X_6]$ and $[B^{3+}X_6]$ octahedra with A^+ cations filling the voids in between.[7] Among the members of this large family of materials, also called *elpasolites*, different compounds, including Cs_2AgBiX_6 (X = Cl, Br, I), $Cs_2AgInCl_6$, $Cs_2NaInCl_6$, $Cs_2NaBiCl_6$, and Cs_2AgSbX_6 (X = Cl, Br) NCs, exhibit interesting PL.[8−15] In particular, $Cs_2AgInCl_6$ has emerged as the most promising double perovskite semiconductor characterized by a direct bandgap. The PL emission from this material is however very weak, because of the parity forbidden nature of the band-edge transition.[16,17] In the past few years, different strategies, including doping and alloying, have been followed to improve the optical properties of $Cs_2AgInCl_6$NCs.[13,18−21] For

Received: August 4, 2020
Accepted: September 28, 2020
Published: September 28, 2020

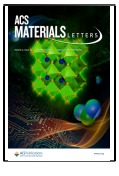

https://dx.doi.org/10.1021/acsmaterialslett.0c00359
ACS Materials Lett. 2020, 2, 1442–1449

instance, doping with either Mn^{2+} or Bi^{3+} ions yielded NCs with an orange emission and a PL quantum yield of 16% or 11%, respectively,[22,23] while doping $Cs_2AgInCl_6$ NCs with rare earth ions made them emitting in the NIR (at ∼1000 nm with Yb^{3+} and at ∼1537 nm with Er^{3+}).[24−26] On the other hand, the systematic replacement of In^{3+} with Bi^{3+} or Ag^+ with Na^+ cations generated alloyed $Cs_2AgIn_xBi_{1-x}Cl_6$ or $Cs_2Ag_{1-x}Na_xInCl_6$ NCs displaying enhanced PL emission.[4,27−31] For example, Yang et al. demonstrated that the bandgap of $Cs_2AgIn_xBi_{1-x}Cl_6$ NCs can be tuned from indirect (x = 0, 0.25, 0.5) to direct (x = 0.75 and 0.9), with NCs of $Cs_2AgIn_{0.9}Bi_{0.1}Cl_6$ composition featuring a PLQY as high as 36%.[31] In another work, Luo et al. obtained Bi-doped $Cs_2Ag_{1-x}Na_xInCl_6$ bulk powders exhibiting a bright white emission with a PLQY of ∼86% for the $Cs_2Ag_{0.6}Na_{0.4}InCl_6$ composition with 1% of Bi dopants, which is currently a record value for double perovskites and makes this specific composition an interesting case study.[4] With the aim of extending such strategies to the nanoscale, in a previous study our group prepared Bi-doped $Cs_2Ag_{1-x}Na_xInCl_6$ NCs displaying a broad yellow emission, with PLQY values of ∼22%.[32] The notable difference in PLQY between bulk powders and colloidal NCs of such DP material is in principle not surprising, considering that surface defects are known to strongly affect the optical properties of both traditional semiconductor and Pb-based perovskite NCs, although the latter to a lesser extent due to the well documented "surface tolerance".[33−36] While our knowledge of the surface passivation of Pb-based perovskite NCs is reaching maturity, we know much less on the ligand shell of double perovskite NCs.[14,37−41] To date, only the ligand shell of $Cs_2AgBiBr_6$ NCs has been examined by Zhang et al., who concluded that the only species passivating the surface are alkylammonium ions.[14]

The identification of surfactants bound to the surface of Bi-doped $Cs_2Ag_{1-x}Na_xInCl_6$ and, more in general, of DP NCs is essential to understand and master their surface chemistry and, consequently, to improve their optical properties. To shed light on this topic, in the present work, we modified the colloidal synthesis of Bi-doped $Cs_2Ag_{1-x}Na_xInCl_6$ NCs to detect via nuclear magnetic resonance (NMR) spectroscopy, the ligand molecules bound to their surface. Our ^{1}H NMR analysis, coupled with nuclear Overhauser effect spectroscopy (NOESY), proved the presence of both carboxylate and alkylammonium species bound and homogeneously intermixed on the surface of the NCs. Also, motivated by these results, we investigated how the size, morphology, and optical properties of Bi-doped $Cs_2Ag_{1-x}Na_xInCl_6$NCs depend on the combination of alkylamines and carboxylic acids with varying chain length used in their synthesis (Scheme 1). Two findings emerged from the study: first, both ligands are essential for the formation of the NCs; second, a variation in the ligand chain length had a minor effect on the size and shape of the NCs, but a more remarkable effect on the PLQY, with the highest value (37%) obtained by using a combination of dodecanoic acid (C12A) and decylamine (C10B) (Scheme 1). Our density functional theory (DFT) calculations indicate that the limited PLQY of this DP NC system can be attributed to unpassivated surface sites, dominated by undercoordinated Cl ions, which even in small amounts result in the formation of deep trap states. The combined experimental and theoretical study reported in this work evidences that halide DPs are much less surface tolerant than the corresponding Pb-based perovskites. Especially in NCs of these materials, a complete passivation of surface trap states might be limited by the steric hindrance of the ligands; therefore, an adequate surface passivation remains an open issue.

Scheme 1. Colloidal Synthesis of Bi-Doped $Cs_2Ag_{1-x}Na_xInCl_6$NCs with Different Ligand Combinations

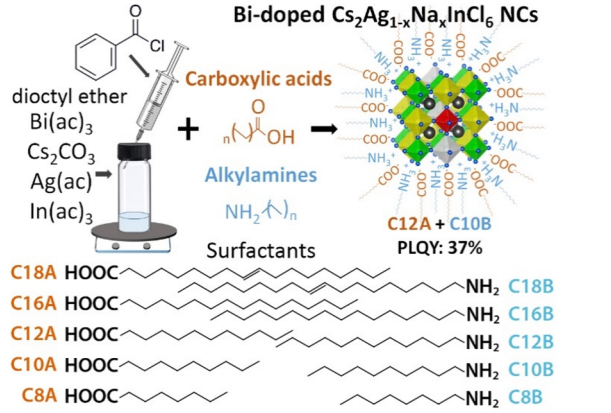

In a typical synthesis of Bi-doped $Cs_2Ag_{1-x}Na_xInCl_6$ NCs, metal acetates, used as cation precursors, are heated in air to the desired reaction temperature (120 °C) in the presence of surfactants and solvent (dioctyl ether) and the reaction is triggered by the swift injection of benzoyl chloride (the halide precursor). Benzoyl halides and acyl halides, in general, are well known for their strong reactivity toward nucleophilic compounds, such as amines and carboxylic acids present in the reaction medium, forming carboxylic acid derivatives even at room temperature (i.e., amides and anhydrides) and simultaneously releasing hydrohalic acids, which are the actual halide precursors triggering the formation of the NCs.[42,43] To vary as few parameters as possible, all the samples reported herein were synthesized by keeping the following fixed: (i) the surfactants/precursors ratio, (ii) the alkylamine/carboxylic acid ratio (i.e., 1/2.1), and (iii) the metal cations/halide precursors' ratio (see the experimental section in the Supporting Information, SI, for details). Under these conditions, we obtain, in all the experiments, NCs containing ∼1% of Bi (with respect to In) and having a mean $Cs_2Ag_{0.6}Na_{0.4}InCl_6$ composition, as confirmed by both inductively coupled plasma optical mass spectrometry (ICP-MS) and scanning electron microscope−energy dispersive X-ray spectroscopy (SEM-EDS) elemental analyses (Table S1). In our syntheses we aimed at this stoichiometry since in previous studies it was found to optimize the optical properties of this system (i.e., highest PLQY).[4,32]

The standard synthesis of both double and Pb-based perovskite NCs relies on a mixture of oleylamine (C18B) and oleic acid (C18A) as surfactants,[12,29,37,43−47] which are characterized by almost overlapping ^{1}H NMR resonances (i.e., alkyl and alkene protons), making it difficult to assess their simultaneous presence on the surface of the NCs.[14,44,48−50] The only protons which could return sufficiently separated signals are those of the CH_2 in position alpha with respect to the COOH and NH_2 groups. Unfortunately, the chemical shift of these protons depends on the relative concentration of both alkyl amine and alkyl carboxylic acid (i.e., on the pH) making their identification not trivial by ^{1}H NMR, especially when they belong to surface bound species, having a broadened signal.[51,52] Thus, here, to unambiguously identify the ligand species bound to the surface of the DP NCs we employed C18B and PhAc in their synthesis. These molecules can be easily distinguished via ^{1}H NMR, as the former is characterized by alkenyl protons, while the latter is characterized by aromatic ones. This combination of ligands yields cubic NCs with a mean size of

https://dx.doi.org/10.1021/acsmaterialslett.0c00359
ACS Materials Lett. 2020, 2, 1442−1449

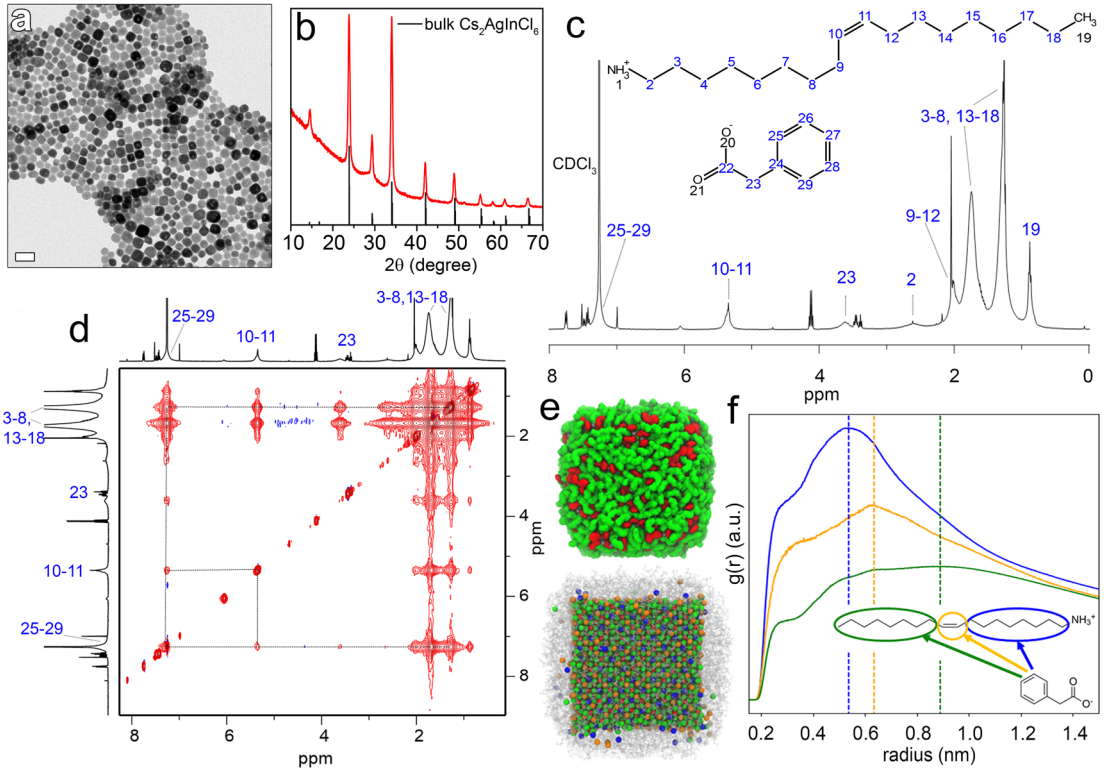

Figure 1. (a) TEM image (scale bar is 50 nm) and (b) XRD pattern of PhAc + C18B NCs. (c) ^{1}H NMR spectrum of PhAc + C18B NCs NCs in $CDCl_3$ and the (d) corresponding ^{1}H−^{1}H NOESY NMR spectrum. (e, top panel) Snapshot from an equilibrated MD simulation at room temperature of a $Cs_2AgInCl_6$ NC capped by PhAc (red molecules, occupying 82% of surface Cl sites) and C18B (green molecules, occupying 54% of surface Cs sites). (e, bottom panel) Stick and ball representation of the snapshot in (e, top panel) of the same colloidal $Cs_2AgInCl_6$ NC in which the inorganic core atoms are represented by colored spheres (Cs, orange; Ag, blue; In, red; Cl, green) and surface ligands by grey lines. (f) Time-average radial distribution function between PhAc aromatic rings and different segments of the C18B alkyl chains: initial aliphatic segments (blue), double bonds (orange), and terminal aliphatic parts (green).

24.4 nm (Figure 1a). On the basis of our XRD analysis, the crystal structure of the NCs matches with the DP $Cs_2AgInCl_6$ structure (ICSD number 244519), and impurity phases are absent (Figure 1b). The NCs feature an absorption peak at 3.7 eV and a PL emission at 2 eV (Figure S1) with a PLQY of 20% (Figure 2b and Table S2), in agreement with our previous work.[32]

These NCs were dispersed in $CDCl_3$ and analyzed by ^{1}H NMR, which indicated that both C18B and PhAc are bound to the NCs' surface (Figure 1c). This is evident from the following observations: (i) the resonances of the CH_2 group close to the amine group (**2**) at 2.6 ppm and of the alkenyl protons (**10**, **11**) at 5.3 ppm are ascribed to C18B, (ii) the proton (**23**) closest to the carboxyl group at 3.6 ppm and the aromatic protons (**25**−**29**) at 7.1 ppm to 7.4 ppm are the footprint of PhAc, and (iii) both C18B and PhAc signals are broadened and shifted with respect to those of free ligands (Figure 1c and Figure S2) indicating the presence of bound species.

The effective anchoring of both surfactants to the surface of double perovskite NCs was corroborated by the ^{1}H−^{1}H NOESY characterization: as can be inferred from the negative sign (red) of the NOESY cross peaks, both PhAc and C18B molecules have longer correlation times (τ_c) with respect to those of the corresponding free ligands (Figures 1d and S3−5 where the sign of the free ligand is positive, blue).[53] Notably, both ligands (PhAc and C18B) show not only intra ligand NOE cross peak interactions, as in the free ligands mixture (Figures S3−5), but also interligand NOE cross peak interactions (Figure 1d). These results indicate that alkylammonium and carboxylate species are proximal to each other, therefore suggesting that they are homogeneously intermixed on the surface of double perovskite NCs (see Figure 1e, upper sketch). To obtain information on the ligand shell composition of our DP NCs, we followed a strategy analogous to a previous one performed on Pb-based perovskite NCs:[54] we dissolved the NCs in dimethyl sulfoxide-d_6 solvent, and subsequently, we acquired a quantitative ^{1}H NMR spectrum (Figure S6), which yielded a PhAc:C18B ratio of bound species of 1.52:1, and a surface ligands density of 4.9 ligands/nm^2. These numbers indicate that ∼52% of Cs surface sites are occupied by oleylammonium cations, and ∼80% of Cl surface sites are occupied by phenyl acetate anions (see SI for details).

To support the NMR results, we carried out MD simulations on a $Cs_2AgInCl_6$ NC model capped by C18B and PhAc ligands (see SI for further info on the force-field employed and the simulations details). The first outcome of our simulations is that within the time scale of the simulation (∼10 nanoseconds) the DP NC surface is able to accommodate both PhAc and C18B ligands in the same experimental concentrations and retain a homogeneously intermixing on the surface, in line with our NOESY results (Figure S7). Additionally, to further elucidate the interaction among the ligands on the surface of the NCs, we also computed the time-average distance between the PhAc aromatic rings and segments of the C18B alkyl chains (Figure 1f). The PhAc aromatic rings peak on-average closer (0.54 nm) to the initial segments of the C18B aliphatic chains (i.e., close to

https://dx.doi.org/10.1021/acsmaterialslett.0c00359
ACS Materials Lett. 2020, 2, 1442−1449

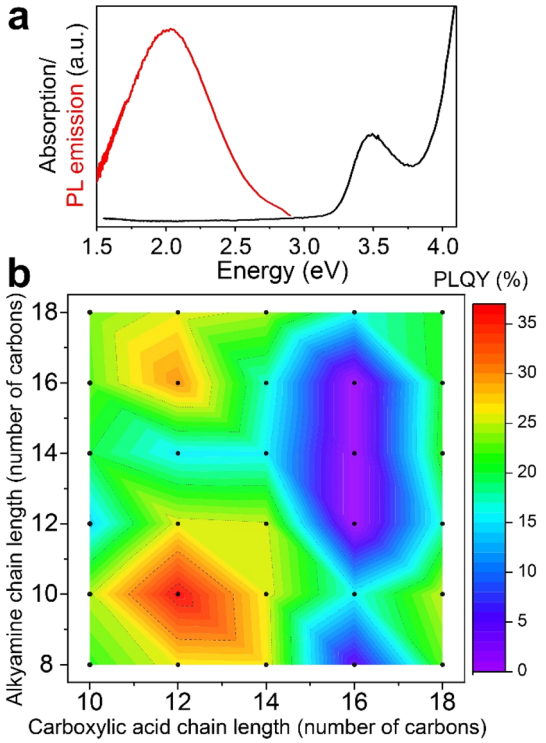

Figure 2. (a) Absorption and PL emission curves of the NC sample obtained with C12A + C10B (i.e., the one with the highest PLQY of 37%). (b) 2D plot of PLQY of DP NCs as a function of the chain length of amines and carboxylic acids employed in the synthesis.

the head of the amines) favoring interactions between these groups. On the other hand, the average distance between PhAc aromatic rings and the terminal segments of the surrounding C18B alkyl chains peak at appreciably higher values (0.63 nm for the alkene bonds and 0.89 nm for terminal aliphatic chains), indicating a weaker interaction among these groups.

These findings, which are substantially different from what observed in $Cs_2AgBiBr_6$ NCs (where akylammonium ions only have been detected),[14] point to a complex ligand shell in which ligands are homogeneously intermixed on the surface of perovskite NCs.

On the basis of our surface characterization, we assumed that the copresence of alkylamines and carboxylic acids in the reaction medium was necessary to stabilize our DP NCs. To prove this hypothesis, we conducted two control experiments in which we employed either oleylamine (C18B) or oleic acid (C18A), a more traditional ligand than PhAc with the same anchoring group, to synthesize the NCs. When employing C18A or C18B only, no NC product could be collected indicating the importance of both surfactants for the formation of the NCs.

To elucidate the role of both alkylamines and carboxylic acids in the synthesis of Bi-doped $Cs_2Ag_{1-x}Na_xInCl_6$ NCs, in analogy to what done with Pb-based perovskite NCs,[49] we ran a series of experiments in which we systematically varied the hydrocarbon chain length of these surfactants (see also Scheme 1) and analyzed the corresponding NC products. The experiments in which combinations of alkylamines and C8A were employed did not yield any solid product. The use of C16A, on the other hand, delivered mostly heavily aggregated products, while in all the other cases colloidal NC with sizes ranging from 8.9 to 23.2 nm were obtained (Figure S8 and Table S2). As emerged from the TEM analysis, there is no clear correlation between the size of the NCs and the chain length of acids and amines employed (Figure S8). The XRD patterns of all the samples are compatible with the expected $Cs_2AgInCl_6$ crystal structure (ICSD number 244519), with no presence of secondary metal halide phases (Figure S9). In some samples the presence of extra XRD peaks is ascribable to crystallized amines or acids (mainly C14A, C16A, C14B, and C16B), which we could not wash away by keeping the same standard cleaning protocol (Figure S9).

The absorption and PL emission curves of all samples are characterized by peaks at ~3.5 and ~2.05 eV, respectively (see representative spectra in Figures 2a and S10). As established in previous works, the excitonic feature observed experimentally in the absorption spectra at ~3.5 eV stems from optically active states within the CB well above the band edge (Figure 3c). Instead, the broad PL band originates from the recombination of electrons and holes localized at the band edges on $BiCl_6$ and $AgCl_6$ octahedra, respectively (Figure 3c).[4,32] These materials feature an optically inactive region close to the lowest edge-to-edge transition with negligible oscillator strength (Figure 3c) resulting in a Stokes shift as large as 1.5 eV.[32]

In our work, the optical properties observed are not much dependent on the chain length of carboxylic acids and alkyl amines employed (Figures 2a and S10). The remarkable difference in optical properties among the different samples is observed in their PLQY, which varies from 0% to 37%, with the highest value achieved when employing C12A + C10B ligands. Figure 2b and Table S2 summarize the PLQY of the various syntheses depending on the combinations of acids and amines that were used.

The strongest emitting DP NCs, that is, those synthesized with C12A + C10B (Figure 2a), were also subjected to ligand exchange procedures with the aim of further increasing their PLQY. In detail, the NCs were treated with different amounts of either Cs-oleate, decyl-, and docecylammonium chloride and bromide, didodecylammonium bromide, didecyldimethylammonium chloride, sodium thiocynate and dodecylbenzenesulfonic acid (Figure S11). In all these tests, we did not observe any increase of the PL emission intensity of the DP NCs, suggesting that no further surface passivation could be achieved by ligand pairs that are commonly employed with Pb-based perovskite NCs.[37,53]

To understand the reasons behind the limited improvements in the PLQY of our DP NCs despite the high surface ligand density detected by NMR, we performed DFT calculations taking as a model system a cubic NC featuring a $Cs_{324}Ag_{65}Na_{43}In_{108}Cl_{756}$ stoichiometry. This corresponds to a diameter of about 3.0 nm and a composition of 60% Ag ions and 40% Na as in the experiments. The Bi^{3+} dopant was not included in the model since it is not expected to influence the surface properties of the NCs. Unlike standard $CsPbBr_3$ NCs, we note that even the fully passivated NC presents strongly localized states at the valence band maximum (VB, Figure 3a). As illustrated in the orbital density plot, these states, although being "shallow", are primarily composed of 3p atomic orbitals on under-coordinated Cl ions at the NC surface (Figure 3a). We, then, proceeded by a step-by-step displacement of CsCl ion pairs surrounding a reference Cl, thus simulating a gradual decapping of the initial perfectly passivated NC surface terminated by CsCl ions. This gradual decapping is shown in Figure 3b on top of each electronic structure plot, and was performed by keeping the reference Cl ion either above a Na or a Ag cation, as we expected a different behavior in each case. As shown in Figure 3b (left panel), the displacement of two CsCl pairs above a Na ion leads

https://dx.doi.org/10.1021/acsmaterialslett.0c00359
ACS Materials Lett. 2020, 2, 1442−1449

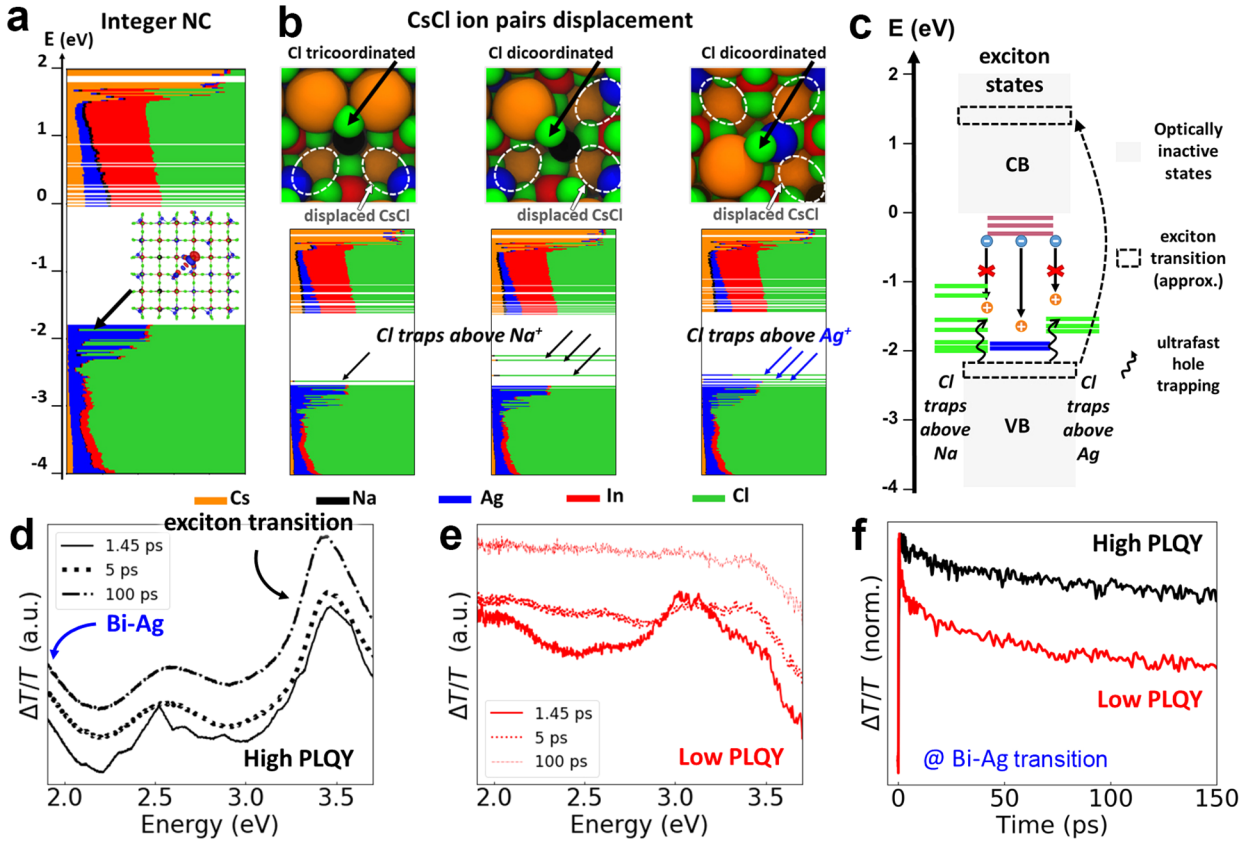

Figure 3. (a) Electronic structure of a ~3.0 nm $Cs_2Ag_{0.60}Na_{0.40}InCl_6$ NC model optimized at the DFT/PBE level of theory, with the relevant contribution of Cl ions (green) to "shallow" trap states inside the valence band. The orbital density plot (inset) reveals a strong localization of these states at the NC surface. (b) Top: Stick and ball view of the most relevant CsCl displacements. Bottom: Emergence of mid-gap states by decreasing the coordination of a surface Cl which lies either above a Na ion (left and middle panels) or above an Ag ion (right panel). (c) Summary of the most important energetic levels involved and the ultrafast hole trapping mechanism which hinders optically active recombination. Transient absorption spectra for representative high (d) and low (e) PLQY samples (37% and 15%, respectively). (f) Pump−probe dynamics of the two samples at the Bi−Ag transition at 1.95 eV.

to the formation of states above the VB. This is even more evident with the displacement of a third CsCl couple that creates several deep states inside the bandgap (Figure 3b, middle panel). This effect is less pronounced when the displacement occurs above an Ag ion, because, unlike Na, the d orbitals of Ag allow the molecular orbitals near the CB edge to be more delocalized, hence more stabilized, throughout the NC (Figure 3b, right panel). It is important to note that the same CsCl displacement in the corresponding Pb-based perovskite ($Cs_{324}Pb_{216}Cl_{756}$ NC model) is much more tolerant to the emergence of mid-gap states, even at the lowest possible coordination (one) of the surface Cl (Figure S12). Overall, our calculation evidence that deep states inside the band gap are easily formed in this material system as a consequence of the nonuniform surface passivation.

Further, to our calculations and to identify the role of carrier trapping at the NCs' surface, we performed transient absorption spectroscopy experiments on two representative samples having a high (~37%, made with C12A + C10B) and low (~15%, made with C10A + C12B) PLQY, respectively (Figure 3d−f). We excited the systems with light pulses with a temporal resolution close to 20 fs in a region well above the bandgap (i.e., 285 nm, 4.35 eV) and probed in a range around 1.90−3.64 eV (340−650 nm), thus covering the most important spectral signatures of the NCs. In this way we were able to follow the carrier recombination after the photoexcitation on relevant time scales. In the transient absorption spectra of the high PLQY sample (Figure 3d), we can clearly identify three main signatures assigned to bleach signals which are due to the ultrafast filling of states after the photoexcitation that overlap with a broad photoinduced absorption (PIA) signal (see SI for more information): (i) a feature at around 3.46 eV (358 nm) is assigned to the main transition involving the electronic states deep in the CB of the DP, also visible in the ground state absorption (Figure 2a and 3c) and (ii) two bands located at around 2.61 eV (475 nm) and 1.95 eV (635 nm), assigned to localized states within the bandgap, the latter ascribable to the $BiCl_6 \rightarrow AgCl_6$ transition responsible for the PL emission of our NCs.[32] The similar rise time of all these bleach signatures of approximately 0.5 ps indicates that they share a common state. When considering the energy level scheme as depicted in Figure 3c this is most probably connected to the VB states, that is, the holes. Notably, in the low PLQY sample (Figure 3e), such features are entirely absent or very weak. Instead, a new and extremely short living feature is observed at ~3.1 eV which we ascribe to the presence of surface trap-related transitions that decay within few picoseconds (Figure S13). The main difference between the two samples analyzed is that the features assigned to the excitonic and Bi−Ag transitions are nearly absent in the low PLQY sample. This can be tentatively explained by considering that, in this sample, the photo-excited holes are immediately trapped by the Cl states above Ag and Na ions. Thus, the main optically active recombination channels that contribute to the

https://dx.doi.org/10.1021/acsmaterialslett.0c00359
ACS Materials Lett. 2020, 2, 1442−1449

emission are suppressed, leading to an overall decrease of the overall PL efficiency. Moreover, if focusing our attention on the decay dynamics of the feature at ~1.95 eV, that is assigned to the localized exciton (Bi−Ag transition), we can observe a much faster recombination rate in the low PLQY sample with respect to the high PLQY sample, in line with the lower efficiency of the former (Figure 3f). Taken together, our transient absorption results indicate that surface hole trapping should play a major role in lowering the PLQY of our NCs by suppressing the efficient localization of holes at the $AgCl_6$ octahedra which are, therefore, absent for the recombination with photoexcited electrons.

In summary, our work has shed light on the surface ligand composition and topology of Bi-doped $Cs_2Ag_{1-x}Na_xInCl_6$ NCs, a double perovskite material system that in the bulk exhibits high PLQY. The combination of various experimental analyses, synthesis optimizations and modeling of both the electronic structure and ligand shell led us to conclude that this material is much less surface tolerant than the corresponding Pb-based perovskites. Therefore, alternative surface passivation strategies for colloidal NCs, for example the epitaxial overgrowth of a shell of another metal halide or chalcogenide material, a standard practice employed to enhance the optical properties of classical II−V and III−V semiconductor NCs, should be sought to further optimize the PLQY of these and, more in general, DP NC systems.

■ ASSOCIATED CONTENT

Supporting Information

The Supporting Information is available free of charge at https://pubs.acs.org/doi/10.1021/acsmaterialslett.0c00359.

Experimental details, SEM-EDS and ICP elemental analyses and size distribution histogram and absorption and PL spectra of Bi-doped $Cs_2Ag_{1-x}Na_xInCl_6$ NCs, ^1H NMR spectra in $CDCl_3$ of mixture of PhAc acid and oleylamine and PhAc + C18B Bi-doped $Cs_2Ag_{1-x}Na_xInCl_6$ NCs, $^1H-^1H$ 2D NOESY spectrum in $CDCl_3$ of mixture of PhAc and oleylamine as free ligands, ^1H NMR and $^1H-^1H$ 2D NOESY spectra in $CDCl_3$ of Bi-doped $Cs_2Ag_{1-x}Na_xInCl_6$ NCs made with PhAc and oleylamine, ^1H NMR spectrum of Bi-doped $Cs_2Ag_{1-x}Na_xInCl_6$ NCs after their dissolution in DMSO-d_6, estimate of the number of surface sites passivated by PhAc and C18B, time-average radial distribution functions, TEM images of Bi-doped $Cs_2Ag_{1-x}Na_xInCl_6$ NCs, XRD patterns of samples obtained with different combinations of alkylamines and carboxylic acids and of hexadecilamine, tetradecylamine, hexadecanoic acid, and tetradecanoic acid, absorption spectra and PL emission curves of Bi-doped $Cs_2Ag_{1-x}Na_xInCl_6$ NCs, PLQY values and mean NC size measured for Bi-doped $Cs_2Ag_{1-x}Na_xInCl_6$ NCs, variation of the PL emission of DP NCs obtained with C12A−C10B and exposed to different ligand pairs, Electronic structure of a ~3.0 nm $Cs_{324}Pb_{216}Cl_{756}$ NC model optimized at the DFT/PBE level of theory, relaxed structure of the NC model illustrating the one-coordinated Cl surrounding, transient absorption spectra for the representative high PLQY sample, and pump−probe dynamics in the first few picoseconds at the three main feature (PDF)

■ AUTHOR INFORMATION

Corresponding Authors

Mengjiao Wang − *Nanochemistry Department, Istituto Italiano di Tecnologia, 16163 Genova, Italy*; Email: mengjiao.wang@iit.it

Ilka Kriegel − *Functional Nanosystems, Istituto Italiano di Tecnologia, 16163 Genova, Italy*; orcid.org/0000-0002-0221-3769; Email: ilka.kriegel@iit.it

Luca De Trizio − *Nanochemistry Department, Istituto Italiano di Tecnologia, 16163 Genova, Italy*; orcid.org/0000-0002-1514-6358; Email: luca.detrizio@iit.it

Liberato Manna − *Nanochemistry Department, Istituto Italiano di Tecnologia, 16163 Genova, Italy*; orcid.org/0000-0003-4386-7985; Email: liberato.manna@iit.it

Authors

Baowei Zhang − *Nanochemistry Department, Istituto Italiano di Tecnologia, 16163 Genova, Italy; Dipartimento di Chimica e Chimica Industriale, Università degli Studi di Genova, 16146 Genova, Italy*

Michele Ghini − *Nanochemistry Department, Istituto Italiano di Tecnologia, 16163 Genova, Italy; Dipartimento di Chimica e Chimica Industriale, Università degli Studi di Genova, 16146 Genova, Italy*

Angela E. M. Melcherts − *Nanochemistry Department, Istituto Italiano di Tecnologia, 16163 Genova, Italy; Debye Institute for Nanomaterials Science, Faculty of Science, Utrecht University, 3584 CC Utrecht, The Netherlands*; orcid.org/0000-0002-5388-7587

Juliette Zito − *Nanochemistry Department, Istituto Italiano di Tecnologia, 16163 Genova, Italy; Dipartimento di Chimica e Chimica Industriale, Università degli Studi di Genova, 16146 Genova, Italy*

Luca Goldoni − *Analytical Chemistry Lab, Istituto Italiano di Tecnologia, 16163 Genova, Italy*

Ivan Infante − *Nanochemistry Department, Istituto Italiano di Tecnologia, 16163 Genova, Italy; Department of Theoretical Chemistry, Vrije Universiteit Amsterdam, 1081 HV Amsterdam, The Netherlands*; orcid.org/0000-0003-3467-9376

Michele Guizzardi − *Dipartimento di Fisica, Politecnico di Milano, 20133 Milano, Italy*

Francesco Scotognella − *Dipartimento di Fisica, Politecnico di Milano, 20133 Milano, Italy*; orcid.org/0000-0003-2781-2116

Complete contact information is available at: https://pubs.acs.org/10.1021/acsmaterialslett.0c00359

Author Contributions

$^{\perp}$B.Z.,M.W., and M.G. contributed equally to this work.

Notes

The authors declare no competing financial interest.

■ ACKNOWLEDGMENTS

We acknowledge S. Lauciello and F. Drago for carrying out SEM-EDS and ICP analyses, respectively. We acknowledge funding from the program for research, Innovation Horizon 2020 (2014−2020) under the Marie Skłodowska-Curie Grant Agreement COMPASS No. 691185 and EPFD0118 CARIPLO 2018. This project has also received funding from the European Research Council Grant Agreement No. 850875 (Light-DYNAMO). The computational work was carried out on the

https://dx.doi.org/10.1021/acsmaterialslett.0c00359
ACS Materials Lett. 2020, 2, 1442−1449

Dutch national e-infrastructure with the support of the SURF Cooperative.

REFERENCES

(1) Yuan, M.; Quan, L. N.; Comin, R.; Walters, G.; Sabatini, R.; Voznyy, O.; Hoogland, S.; Zhao, Y.; Beauregard, E. M.; Kanjanaboos, P.; Lu, Z.; Kim, D. H.; Sargent, E. H. Perovskite Energy Funnels for Efficient Light-Emitting Diodes. *Nat. Nanotechnol.* **2016**, *11*, 872−877.

(2) Akkerman, Q. A.; Rainò, G.; Kovalenko, M. V.; Manna, L. Genesis, Challenges and Opportunities for Colloidal Lead Halide Perovskite Nanocrystals. *Nat. Mater.* **2018**, *17*, 394−405.

(3) He, X.; Qiu, Y.; Yang, S. Fully-Inorganic Trihalide Perovskite Nanocrystals: A New Research Frontier of Optoelectronic Materials. *Adv. Mater.* **2017**, *29*, 1700775.

(4) Luo, J.; Wang, X.; Li, S.; Liu, J.; Guo, Y.; Niu, G.; Yao, L.; Fu, Y.; Gao, L.; Dong, Q.; Zhao, C.; Leng, M.; Ma, F.; Liang, W.; Wang, L.; Jin, S.; Han, J.; Zhang, L.; Etheridge, J.; Wang, J.; Yan, Y.; Sargent, E. H.; Tang, J. Efficient and Stable Emission of Warm-White Light from Lead-Free Halide Double Perovskites. *Nature* **2018**, *563*, 541−545.

(5) Song, Z.; Shrestha, N.; Watthage, S. C.; Liyanage, G. K.; Almutawah, Z. S.; Ahangharnejhad, R. H.; Phillips, A. B.; Ellingson, R. J.; Heben, M. J. Impact of Moisture on Photoexcited Charge Carrier Dynamics in Methylammonium Lead Halide Perovskites. *J. Phys. Chem. Lett.* **2018**, *9*, 6312−6320.

(6) Leng, M.; Chen, Z.; Yang, Y.; Li, Z.; Zeng, K.; Li, K.; Niu, G.; He, Y.; Zhou, Q.; Tang, J. Lead-Free, Blue Emitting Bismuth Halide Perovskite Quantum Dots. *Angew. Chem., Int. Ed.* **2016**, *55*, 15012−15016.

(7) Filip, M. R.; Hillman, S.; Haghighirad, A. A.; Snaith, H. J.; Giustino, F. Band Gaps of the Lead-Free Halide Double Perovskites $Cs_2BiAgCl_6$ and $Cs_2BiAgBr_6$ from Theory and Experiment. *J. Phys. Chem. Lett.* **2016**, *7*, 2579−2585.

(8) Vasala, S.; Karppinen, M. $A_2B'B''O_6$ Perovskites: A Review. *Prog. Solid State Chem.* **2015**, *43*, 1−36.

(9) Xuan, T.; Xie, R.-J. Recent Processes on Light-Emitting Lead-Free Metal Halide Perovskites. *Chem. Eng. J.* **2020**, *393*, 124757.

(10) Pham, H. Q.; Holmes, R. J.; Aydil, E. S.; Gagliardi, L. Lead-Free Double Perovskites $Cs_2InCuCl_6$ and $(CH_3NH_3)_2InCuCl_6$: Electronic, Optical, and Electrical Properties. *Nanoscale* **2019**, *11*, 11173−11182.

(11) Lv, K.; Qi, S.; Liu, G.; Lou, Y.; Chen, J.; Zhao, Y. Lead-Free Silver-Antimony Halide Double Perovskite Quantum Dots with Superior Blue Photoluminescence. *Chem. Commun. (Cambridge, U. K.)* **2019**, *55*, 14741−14744.

(12) Dahl, J. C.; Osowiecki, W. T.; Cai, Y.; Swabeck, J. K.; Bekenstein, Y.; Asta, M.; Chan, E. M.; Alivisatos, A. P. Probing the Stability and Band Gaps of $Cs_2AgInCl_6$ and $Cs_2AgSbCl_6$ Lead-Free Double Perovskite Nanocrystals. *Chem. Mater.* **2019**, *31*, 3134−3143.

(13) Zhou, J.; Rong, X.; Zhang, P.; Molokeev, M. S.; Wei, P.; Liu, Q.; Zhang, X.; Xia, Z. Manipulation of Bi^{3+}/In^{3+} Transmutation and Mn^{2+}-Doping Effect on the Structure and Optical Properties of Double Perovskite $Cs_2NaBi_{1-x}In_xCl_6$. *Adv. Opt. Mater.* **2019**, *7*, 1801435.

(14) Zhang, Y.; Shah, T.; Deepak, F. L.; Korgel, B. A. Surface Science and Colloidal Stability of Double-Perovskite $Cs_2AgBiBr_6$ Nanocrystals and Their Superlattices. *Chem. Mater.* **2019**, *31*, 7962−7969.

(15) Yang, D.; Li, X.; Zhou, W.; Zhang, S.; Meng, C.; Wu, Y.; Wang, Y.; Zeng, H. $CsPbBr_3$ Quantum Dots 2.0: Benzenesulfonic Acid Equivalent Ligand Awakens Complete Purification. *Adv. Mater.* **2019**, *0*, 1900767.

(16) Luo, J.; Li, S.; Wu, H.; Zhou, Y.; Li, Y.; Liu, J.; Li, J.; Li, K.; Yi, F.; Niu, G.; Tang, J. $Cs_2AgInCl_6$ Double Perovskite Single Crystals: Parity Forbidden Transitions and Their Application for Sensitive and Fast Uv Photodetectors. *ACS Photonics* **2018**, *5*, 398−405.

(17) Meng, W.; Wang, X.; Xiao, Z.; Wang, J.; Mitzi, D. B.; Yan, Y. Parity-Forbidden Transitions and Their Impact on the Optical Absorption Properties of Lead-Free Metal Halide Perovskites and Double Perovskites. *J. Phys. Chem. Lett.* **2017**, *8*, 2999−3007.

(18) Zhao, F.; Song, Z.; Zhao, J.; Liu, Q. Double Perovskite $Cs_2AgInCl_6$:Cr^{3+}: Broadband and near-Infrared Luminescent Materials. *Inorg. Chem. Front.* **2019**, *6*, 3621−3628.

(19) Dave, K.; Fang, M. H.; Bao, Z.; Fu, H. T.; Liu, R. S. Recent Developments in Lead-Free Double Perovskites: Structure, Doping, and Applications. *Chem. - Asian J.* **2020**, *15*, 242−252.

(20) Zhao, X.-G.; Yang, D.; Ren, J.-C.; Sun, Y.; Xiao, Z.; Zhang, L. Rational Design of Halide Double Perovskites for Optoelectronic Applications. *Joule* **2018**, *2*, 1662−1673.

(21) Chen, N.; Cai, T.; Li, W.; Hills-Kimball, K.; Yang, H.; Que, M.; Nagaoka, Y.; Liu, Z.; Yang, D.; Dong, A.; Xu, C. Y.; Zia, R.; Chen, O. Yb- and Mn-Doped Lead-Free Double Perovskite Cs_2AgBiX_6 ($X = Cl^-$, Br^-) Nanocrystals. *ACS Appl. Mater. Interfaces* **2019**, *11*, 16855−16863.

(22) Locardi, F.; Cirignano, M.; Baranov, D.; Dang, Z.; Prato, M.; Drago, F.; Ferretti, M.; Pinchetti, V.; Fanciulli, M.; Brovelli, S.; De Trizio, L.; Manna, L. Colloidal Synthesis of Double Perovskite $Cs_2AgInCl_6$ and Mn-Doped $Cs_2AgInCl_6$ Nanocrystals. *J. Am. Chem. Soc.* **2018**, *140*, 12989−12995.

(23) Liu, Y.; Jing, Y.; Zhao, J.; Liu, Q.; Xia, Z. Design Optimization of Lead-Free Perovskite $Cs_2AgInCl_6$:Bi Nanocrystals with 11.4% Photoluminescence Quantum Yield. *Chem. Mater.* **2019**, *31*, 3333−3339.

(24) Lee, W.; Hong, S.; Kim, S. Colloidal Synthesis of Lead-Free Silver-Indium Double-Perovskite $Cs_2AgInCl_6$ Nanocrystals and Their Doping with Lanthanide Ions. *J. Phys. Chem. C* **2019**, *123*, 2665−2672.

(25) Mahor, Y.; Mir, W. J.; Nag, A. Synthesis and Near-Infrared Emission of Yb-Doped $Cs_2AgInCl_6$ Double Perovskite Microcrystals and Nanocrystals. *J. Phys. Chem. C* **2019**, *123*, 15787−15793.

(26) Arfin, H.; Kaur, J.; Sheikh, T.; Chakraborty, S.; Nag, A. Bi^{3+}-Er^{3+} and Bi^{3+}-Yb^{3+} Codoped $Cs_2AgInCl_6$ Double Perovskite near-Infrared Emitters. *Angew. Chem., Int. Ed.* **2020**, *59*, 11307−11311.

(27) Du, K. Z.; Meng, W.; Wang, X.; Yan, Y.; Mitzi, D. B. Bandgap Engineering of Lead-Free Double Perovskite $Cs_2AgBiBr_6$ through Trivalent Metal Alloying. *Angew. Chem., Int. Ed.* **2017**, *56*, 8158−8162.

(28) Tran, T. T.; Panella, J. R.; Chamorro, J. R.; Morey, J. R.; McQueen, T. M. Designing Indirect-Direct Bandgap Transitions in Double Perovskites. *Mater. Horiz.* **2017**, *4*, 688−693.

(29) Manna, D.; Das, T. K.; Yella, A. Tunable and Stable White Light Emission in Bi^{3+}-Alloyed $Cs_2AgInCl_6$ Double Perovskite Nanocrystals. *Chem. Mater.* **2019**, *31*, 10063−10070.

(30) Gray, M. B.; Majher, J. D.; Strom, T. A.; Woodward, P. M. Broadband White Emission in $Cs_2AgIn_{1-x}Bi_xCl_6$ Phosphors. *Inorg. Chem.* **2019**, *58*, 13403−13410.

(31) Yang, B.; Mao, X.; Hong, F.; Meng, W.; Tang, Y.; Xia, X.; Yang, S.; Deng, W.; Han, K. Lead-Free Direct Band Gap Double-Perovskite Nanocrystals with Bright Dual-Color Emission. *J. Am. Chem. Soc.* **2018**, *140*, 17001−17006.

(32) Locardi, F.; Sartori, E.; Buha, J.; Zito, J.; Prato, M.; Pinchetti, V.; Zaffalon, M. L.; Ferretti, M.; Brovelli, S.; Infante, I.; De Trizio, L.; Manna, L. Emissive Bi-Doped Double Perovskite $Cs_2Ag_{1-x}Na_xInCl_6$ Nanocrystals. *ACS Energy Lett.* **2019**, *4*, 1976−1982.

(33) Peng, W.; Anand, B.; Liu, L.; Sampat, S.; Bearden, B. E.; Malko, A. V.; Chabal, Y. J. Influence of Growth Temperature on Bulk and Surface Defects in Hybrid Lead Halide Perovskite Films. *Nanoscale* **2016**, *8*, 1627−34.

(34) Zheng, X.; Chen, B.; Dai, J.; Fang, Y.; Bai, Y.; Lin, Y.; Wei, H.; Zeng, X. C.; Huang, J. Defect Passivation in Hybrid Perovskite Solar Cells Using Quaternary Ammonium Halide Anions And cations. *Nat. Energy* **2017**, *2*, 17102.

(35) Bohn, B. J.; Tong, Y.; Gramlich, M.; Lai, M. L.; Doblinger, M.; Wang, K.; Hoye, R. L. Z.; Muller-Buschbaum, P.; Stranks, S. D.; Urban, A. S.; Polavarapu, L.; Feldmann, J. Boosting Tunable Blue Luminescence of Halide Perovskite Nanoplatelets through Postsynthetic Surface Trap Repair. *Nano Lett.* **2018**, *18*, 5231−5238.

(36) Barker, A. J.; Sadhanala, A.; Deschler, F.; Gandini, M.; Senanayak, S. P.; Pearce, P. M.; Mosconi, E.; Pearson, A. J.; Wu, Y.; Srimath Kandada, A. R.; Leijtens, T.; De Angelis, F.; Dutton, S. E.; Petrozza, A.; Friend, R. H. Defect-Assisted Photoinduced Halide Segregation in Mixed-Halide Perovskite Thin Films. *ACS Energy Lett.* **2017**, *2*, 1416−1424.

(37) Shamsi, J.; Urban, A. S.; Imran, M.; De Trizio, L.; Manna, L. Metal Halide Perovskite Nanocrystals: Synthesis, Post-Synthesis

https://dx.doi.org/10.1021/acsmaterialslett.0c00359
ACS Materials Lett. 2020, 2, 1442−1449

Modifications, and Their Optical Properties. *Chem. Rev.* **2019**, *119*, 3296−3348.
(38) ten Brinck, S.; Zaccaria, F.; Infante, I. Defects in Lead Halide Perovskite Nanocrystals: Analogies and (Many) Differences with the Bulk. *ACS Energy Lett.* **2019**, *4*, 2739−2747.
(39) Yang, D.; Li, X.; Zeng, H. Surface Chemistry of All Inorganic Halide Perovskite Nanocrystals: Passivation Mechanism and Stability. *Adv. Mater. Interfaces* **2018**, *5*, 1701662.
(40) Yang, D.; Cao, M.; Zhong, Q.; Li, P.; Zhang, X.; Zhang, Q. All-Inorganic Cesium Lead Halide Perovskite Nanocrystals: Synthesis, Surface Engineering and Applications. *J. Mater. Chem. C* **2019**, *7*, 757−789.
(41) Zhang, Y.; Siegler, T. D.; Thomas, C. J.; Abney, M. K.; Shah, T.; De Gorostiza, A.; Greene, R. M.; Korgel, B. A. A "Tips and Tricks" Practical Guide to the Synthesis of Metal Halide Perovskite Nanocrystals. *Chem. Mater.* **2020**, *32*, 5410−5423.
(42) Patai, S. *The Chemistry of Acyl Halides*; John Wiley & Sons, Ltd.: UK, 1972.
(43) Imran, M.; Caligiuri, V.; Wang, M.; Goldoni, L.; Prato, M.; Krahne, R.; De Trizio, L.; Manna, L. Benzoyl Halides as Alternative Precursors for the Colloidal Synthesis of Lead-Based Halide Perovskite Nanocrystals. *J. Am. Chem. Soc.* **2018**, *140*, 2656−2664.
(44) De Roo, J.; Ibáñez, M.; Geiregat, P.; Nedelcu, G.; Walravens, W.; Maes, J.; Martins, J. C.; Van Driessche, I.; Kovalenko, M. V.; Hens, Z. Highly Dynamic Ligand Binding and Light Absorption Coefficient of Cesium Lead Bromide Perovskite Nanocrystals. *ACS Nano* **2016**, *10*, 2071−2081.
(45) Han, P.; Zhang, X.; Mao, X.; Yang, B.; Yang, S.; Feng, Z.; Wei, D.; Deng, W.; Pullerits, T.; Han, K. Size Effect of Lead-Free Halide Double Perovskite on Luminescence Property. *Sci. China: Chem.* **2019**, *62*, 1405−1413.
(46) Lamba, R. S.; Basera, P.; Bhattacharya, S.; Sapra, S. Band Gap Engineering in $Cs_2(Na_xAg_{1-x})BiCl_6$ Double Perovskite Nanocrystals. *J. Phys. Chem. Lett.* **2019**, *10*, 5173−5181.
(47) Yao, M. M.; Wang, L.; Yao, J. S.; Wang, K. H.; Chen, C.; Zhu, B. S.; Yang, J. N.; Wang, J. J.; Xu, W. P.; Zhang, Q.; Yao, H. B. Improving Lead-Free Double Perovskite $Cs_2NaBiCl_6$ Nanocrystal Optical Properties Via Ion Doping. *Adv. Opt. Mater.* **2020**, *8*, 1901919.
(48) Yoo, D.; Woo, J. Y.; Kim, Y.; Kim, S. W.; Wei, S. H.; Jeong, S.; Kim, Y. H. Origin of the Stability and Transition from Anionic to Cationic Surface Ligand Passivation of All-Inorganic Cesium Lead Halide Perovskite Nanocrystals. *J. Phys. Chem. Lett.* **2020**, *11*, 652−658.
(49) Pan, A.; He, B.; Fan, X.; Liu, Z.; Urban, J. J.; Alivisatos, A. P.; He, L.; Liu, Y. Insight into the Ligand-Mediated Synthesis of Colloidal $CsPbBr_3$ Perovskite Nanocrystals: The Role of Organic Acid, Base, and Cesium Precursors. *ACS Nano* **2016**, *10*, 7943−7954.
(50) Smock, S. R.; Williams, T. J.; Brutchey, R. L. Quantifying the Thermodynamics of Ligand Binding to $CsPbBr_3$ Quantum Dots. *Angew. Chem., Int. Ed.* **2018**, *57*, 11711−11715.
(51) Almeida, G.; Goldoni, L.; Akkerman, Q.; Dang, Z.; Khan, A. H.; Marras, S.; Moreels, I.; Manna, L. Role of Acid-Base Equilibria in the Size, Shape, and Phase Control of Cesium Lead Bromide Nanocrystals. *ACS Nano* **2018**, *12*, 1704−1711.
(52) Almeida, G.; Goldoni, L.; Akkerman, Q.; Dang, Z.; Khan, A. H.; Marras, S.; Moreels, I.; Manna, L. Role of Acid-Base Equilibria in the Size, Shape, and Phase Control of Cesium Lead Bromide Nanocrystals. *ACS Nano* **2018**, *12*, 1704−1711.
(53) Nenon, D. P.; Pressler, K.; Kang, J.; Koscher, B. A.; Olshansky, J. H.; Osowiecki, W. T.; Koc, M. A.; Wang, L.-W.; Alivisatos, A. P. Design Principles for Trap-Free $CsPbX_3$ Nanocrystals: Enumerating and Eliminating Surface Halide Vacancies with Softer Lewis Bases. *J. Am. Chem. Soc.* **2018**, *140*, 17760−17772.
(54) Almeida, G.; Ashton, O. J.; Goldoni, L.; Maggioni, D.; Petralanda, U.; Mishra, N.; Akkerman, Q. A.; Infante, I.; Snaith, H. J.; Manna, L. The Phosphine Oxide Route toward Lead Halide Perovskite Nanocrystals. *J. Am. Chem. Soc.* **2018**, *140*, 14878−14886.

https://dx.doi.org/10.1021/acsmaterialslett.0c00359
ACS Materials Lett. 2020, 2, 1442−1449